CARAVEL

Publish open access at Caravel Press

Green Technology & Innovation

Journal homepage: gtijournal.com

Technical article

Self-powered and self-purifying building envelopes: Progress, challenges, and future perspectives

Yu Qian [1], Jie Ji [1]*, Suyue Xu [1], Yifei Gao [1], Ziheng Li [1], Hengmin Jia [2], and Yan Mu [2]

[1] *Department of Thermal Science and Energy Engineering, University of Science and Technology of China, Hefei 230026, China.*
[2] *Department of Infection Control, the First Affiliated Hospital of USTC, Division of Life Sciences and Medicine, University of Science and Technology of China, Hefei 230026, China.*

A B S T R A C T

Self-powered and self-purifying building envelopes enable the simultaneous utilization of renewable energy and indoor air purification without external energy input, offering dual benefits in reducing building energy consumption and improving indoor air quality. This concept aligns well with the post-pandemic demand for integrated strategies addressing both building energy efficiency and bioaerosol control. In recent years, preliminary progress has been made in terms of technical pathway exploration and system feasibility demonstration. However, existing studies remain largely fragmented, and a comprehensive and systematic review of the research landscape and key scientific challenges is still lacking. This paper presents a systematic review of recent advances in self-powered and self-purifying building envelopes, with a particular focus on three aspects: microbial inactivation mechanisms, system modeling approaches, and system optimization strategies. Based on the reviewed literature, future research directions are further summarized and discussed, including the development of bacterial and viral multi-parameter inactivation models under coupled environmental parameters (e.g., temperature, humidity, and ultraviolet irradiation), the advancement of multi-level modeling and solution frameworks to balance computational efficiency and physical fidelity, and the systematic evaluation of system applicability across different climate zones and building types to elucidate the synergistic mechanisms between system configuration and operational optimization. This review aims to provide a unified research framework and reference for mechanism studies, model development, and system design of self-powered and self-purifying building envelopes, thereby supporting their further technological development and practical implementation.

A R T I C L E I N F O

Article History:
Received: 02 February 2026
Revised: 20 February 2026
Accepted: 03 March 2026

Keywords:
Solar energy
Multi-functional energy utilization
Air purification
Bioaerosol
Thermal disinfection
BIPVT

Article Citation:
Qian, Y., Ji Jie, Xu, S., Gao, Y., Li, Z., Jia, H., & Mu, Y. (2026). Self-powered and self-purifying building envelopes: Progress, challenges, and future perspectives. Green Technology & Innovation, 2(1), 62–85.
https://doi.org/10.65582/gti.2026.005

1. INTRODUCTION

With rapid economic development and accelerating urbanization, building energy demand continues to increase. Studies indicate that building operation accounts for approximately 30% of global final energy consumption, while the associated carbon dioxide emissions contribute about 26% of total global CO2 emissions (Yu et al., 2024). Energy use during building operation mainly arises from lighting, heating,

* Corresponding author. Email address: jijie@ustc.edu.cn (Jie Ji)

ventilation and air conditioning, domestic hot water, cooking, and office equipment, among which heating, ventilation, and air conditioning (HVAC) systems typically account for 30-50% of total operational energy consumption (Torres et al., 2020). Therefore, reducing HVAC energy use is one of the key pathways to achieving energy conservation and emission reduction in the building sector. As a widely distributed, abundant, and readily accessible renewable energy source that can be easily integrated into buildings, solar energy enables building-integrated photovoltaic thermal (BIPVT) envelopes, providing a promising solution for reducing HVAC energy demand and promoting low-carbon building operation (Ke et al., 2021a). From a techno-economic perspective, BIPVT systems can simultaneously generate electricity and useful thermal energy from the same collector area, which improves overall solar utilization efficiency and can shorten the energy payback period compared with conventional PV systems. Several studies have shown that the integration of PV/T collectors into building envelopes can reduce both operational energy consumption and lifecycle carbon emissions while providing additional economic benefits through on-site energy production (Chow, 2018, Herrando et al., 2014, Asaee et al., 2017).

Meanwhile, indoor bioaerosol pollution caused by bacterial growth and the release of external pathogens, such as coronaviruses, has become increasingly prominent. For example, the outbreak of coronavirus disease 2019 (COVID-19) demonstrated that severe acute respiratory syndrome coronavirus 2 (SARS-CoV-2) can be transmitted via aerosols in poorly ventilated and densely occupied indoor environments, leading to large-scale infections (Liu et al., 2020). According to statistics, the COVID-19 pandemic resulted in approximately 14.83 million excess deaths worldwide (Msemburi et al., 2023). Against this backdrop, the development of indoor bioaerosol control technologies that are both energy-efficient and highly effective has become a major research focus. Thermal disinfection achieves efficient microbial inactivation by disrupting cellular structures, proteins, and genetic material through elevated temperatures (Vlaskin, 2022). Compared with other air purification technologies, thermal treatment of indoor air does not generate harmful by-products such as ozone and is therefore considered a safe and reliable purification method (Song et al., 2022); however, its relatively high energy consumption has limited widespread application in buildings.

Notably, in BIPVT, appropriate system design and operational optimization can enable the internal air temperature of the envelope to reach approximately 80 °C without additional energy input (Zhao et al., 2017), thereby partially overcoming the high energy demand associated with conventional thermal disinfection technologies. Consequently, integrating BIPVT technology with thermal disinfection mechanisms to develop self-powered and self-purifying building envelopes offers a clean, efficient, and sustainable pathway to simultaneously achieve building energy savings, carbon emission reduction, and indoor bioaerosol control. Focusing on this emerging type of building envelope, this paper discusses the evolution of bioaerosol thermal inactivation behavior, the coupled thermal-electrical-purification mechanisms within the envelope, as well as system construction and optimization strategies, summarizes current research progress, identifies key challenges, and outlines future research directions.

This review focuses on self-sustained, self-purifying building envelopes. Literature was primarily retrieved from Web of Science, Scopus, and Google Scholar using combined keywords such as “BIPVT / PVT / Trombe wall / building envelope” and “air purification / disinfection / bioaerosol”. We included studies that are highly relevant to the topic and that provide clear technical pathways or quantifiable purification/disinfection performance metrics, thereby forming the core body of literature and the review framework of this paper.

2. THERMAL INACTIVATION OF BACTERIAL AEROSOL

Self-powered and self-purifying building envelopes primarily rely on microbial thermal inactivation to achieve air purification; therefore, elucidating the thermal inactivation behavior and its evolution for pathogenic bioaerosols is a fundamental prerequisite for the development of such systems. Jung et al. (Jung et al., 2009) designed a continuous-flow heating device in which bacterial bioaerosols passed through a quartz tube externally wrapped with heating coils, with a residence time of approximately 0.3s. At wall temperatures of 160°C and 350°C, more than 99.9% inactivation of Escherichia coli and Bacillus subtilis, respectively, was achieved. Mullican et al. (Mullican et al., 1971) developed a heated mixing device that enabled rapid temperature elevation through mixing heated air with bacterial aerosols. Their results showed that at a residence time of approximately 0.02 s, no significant inactivation of Bacillus subtilis occurred when the mixed temperature was below 204°C, whereas near-complete inactivation was observed when the temperature increased to 260°C. Liu et al. (Liu et al., 2023b) employed electromagnetically heated coils to evaluate the

thermal resistance of Bacillus subtilis spores, demonstrating that a residence time of approximately 1s combined with an outlet temperature of 250°C resulted in around 99.9% bacterial inactivation.

It should be noted that most of the aforementioned studies are confined to sub-second residence time scales, which necessitate relatively high temperatures for effective inactivation. Maintaining such high-temperature conditions leads to substantial energy consumption, thereby limiting the practical application of thermal inactivation technologies in building environments. To address this limitation, Xie et al. (Xie et al., 2024b) further investigated the thermal resistance of bioaerosols under temperature and time scales relevant to solar air-heating systems, with the experimental setup illustrated in Fig. 1(a). By maintaining constant air temperature and flow rate within the inactivation tube, various combinations of exposure temperature and residence time for different bioaerosols could be achieved. Measurements of bioaerosol concentrations at the inlet and outlet of the tube enabled the determination of survival fractions and the characterization of bacterial thermal inactivation curves. Bacterial inactivation processes are commonly described using several models, including the first-order kinetic model (Xiong et al., 1999), the Weibull model (van Boekel, 2002), and the biphasic model (Phaiboun et al., 2015). Among these, the first-order kinetic model is most widely applied, and the temperature dependence of the inactivation rate constant is typically described using the Arrhenius equation.

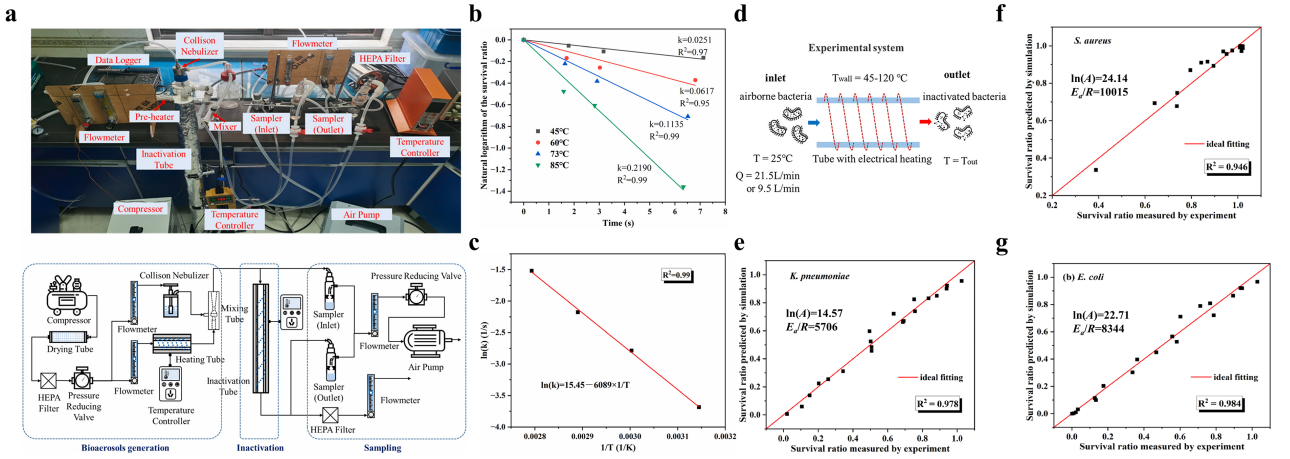

Figure 1. Experimental study on thermal inactivation of bacterial aerosols. **(a)** Schematic diagram and photograph of the continuous-flow experimental setup; **(b)** Temperature-dependent thermal inactivation rate constants obtained from isothermal experiments; **(c)** Arrhenius-law fitting results based on isothermal experiments; **(d)** Schematic illustration of the non-isothermal experimental protocol; **(e)** Arrhenius-law fitting results for K. pneumoniae derived from non-isothermal experiments; **(f)** Arrhenius-law fitting results for S. aureus derived from non-isothermal experiments; **(g)** Arrhenius-law fitting results for E. coli derived from non-isothermal experiments.

$$\frac{dC}{dt} = -kC \tag{1}$$

$$k = Aexp\left(-\frac{E_a}{RT}\right) \tag{2}$$

Taking Klebsiella pneumoniae as an example, the first-order inactivation rate constants (k) at different temperatures are shown in Fig. 1(b), and the corresponding k-T relationship derived from the Arrhenius law is presented in Fig. 1(c). However, in practical building envelope systems, airflow within channels is generally subjected to a continuous heating process rather than isothermal conditions. In addition, under high-temperature isothermal inactivation conditions, bacterial aerosols may undergo premature inactivation due to mixing with high-temperature dilution air prior to entering the inactivation tube, leading to reduced inlet concentrations and compromised representativeness of measured survival fractions. In light of these considerations, Xie et al. (Xie et al., 2024a) conducted variable-temperature inactivation experiments on different bacterial aerosols. In these experiments, the inlet air temperature was maintained at 25°C, while the wall temperature was adjusted to 45°C, 60°C, 80°C, 100°C, and 120°C, respectively, as shown in Fig. 1(d), to examine bacterial survival during realistic heating processes. Furthermore, a CFD model was established to characterize the non-isothermal process within the inactivation tube, and particle swarm optimization was

employed to identify the thermal inactivation kinetic parameters. Comparisons between the fitted results and experimental data are presented in Fig. 1(e-g).

Although thermal inactivation kinetic models of bioaerosols under different temperature and residence time conditions have been established, these models primarily account for temperature effects alone. In practice, additional environmental parameters such as humidity and ultraviolet irradiance can also significantly influence bioaerosol inactivation, and the inactivation behavior under multi-parameter coupled conditions remains insufficiently understood. Moreover, existing experimental studies have predominantly focused on bacteria, while the multi-parameter inactivation behavior of viral bioaerosols requires further investigation.

The mechanistic insights summarized above clarify what drives bioaerosol removal and inactivation within self-powered and self-purifying envelopes. To move from qualitative understanding to quantitative evaluation, these mechanisms must be translated into predictive models that can resolve the coupled heat transfer, airflow, and bioaerosol transport processes under realistic boundary conditions. This motivates the modeling approaches introduced in the following section.

3. MODELING AND SOLUTION OF THE COUPLED LIGHT-ELECTRICAL-THERMAL-PURIFICATION PROCESS

3.1. WORK PRINCIPLE

In self-powered and self-purifying building envelopes, light-electrical-thermal-purification processes are intrinsically coupled, involving multiple physical and biological phenomena such as radiation absorption, electrical energy conversion, heat and mass transfer, and microbial inactivation. As a result, the modeling and solution of such systems exhibit pronounced multi-scale and multi-physics characteristics. For system-level numerical performance evaluation and parametric analysis, existing studies generally adopt two categories of modeling approaches: one is low-dimensional numerical models with streamwise discretization for rapid system-level assessment, and the other is high-dimensional numerical models with spatial resolution. In the following, these two modeling approaches are introduced based on a representative self-powered and self-purifying wall-type building envelope.

Fig. 2(a) illustrates a typical self-powered and self-purifying wall envelope, which consists, from the exterior to the interior, of a glass cover, an enclosed air gap, a photovoltaic (PV) absorber plate, an air channel, a back plate, an insulation layer, and the wall (Xie et al., 2021). When solar radiation is incident on the system surface, most of the incoming solar energy passes through the glass cover and impinges on the PV absorber plate. A portion of the absorbed energy is converted into electrical power through the photovoltaic effect, while the remaining part is absorbed as thermal energy, leading to an increase in the temperature of the PV cells and the absorber plate. The temperature difference between the absorber plate and the air within the channel induces a thermosiphon effect, whereby indoor air is continuously drawn into the air channel through the lower inlet, heated via natural convection, and then returned to the indoor space through the upper outlet. Through this cyclic process, passive space heating is achieved. During operation, the photovoltaic cells are cooled, thereby enhancing electrical conversion efficiency; simultaneously, bacteria-laden indoor air is repeatedly exposed to elevated temperatures, promoting protein denaturation and enabling thermal disinfection.

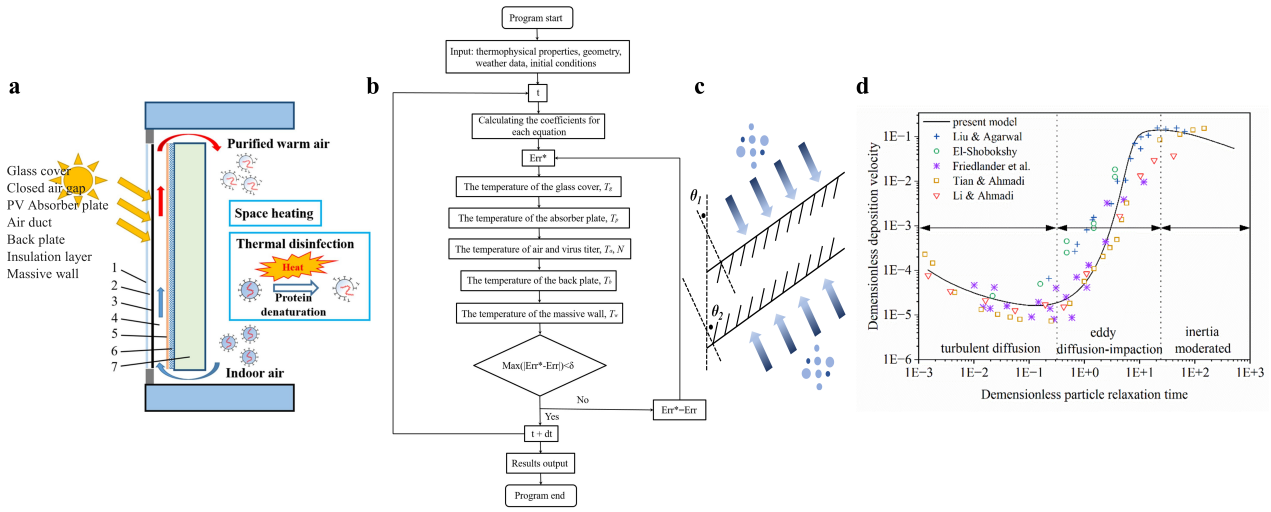

Figure 2. Modeling and solution of a typical self-powered and self-purifying wall-type building envelop. **(a)** Schematic diagram of a typical self-powered and self-purifying wall-type building envelop; **(b)** Simulation workflow of a low-dimensional numerical model based on streamwise discretization; **(c)** Schematic illustration of particle deposition onto an inclined wall; **(d)** Dimensionless deposition velocity of particles with different relaxation times.

3.2. STREAMWISE LOW-DIMENSIONAL MODEL

For simplified reduced-order models, energy and mass conservation equations are established to couple key variables such as solar irradiance, component temperatures, air temperature, airflow velocity, and bioaerosol concentration, enabling rapid prediction of the overall system behavior. Specifically, energy balance equations are formulated for the glass cover, the PV absorber plate, the air within the channel, the back plate, the wall, and the indoor air, as expressed as follows (Ke et al., 2021b):

For the glass cover:

$$\rho_g \delta_g c_g \frac{\partial T_g}{\partial t} = \lambda_g \delta_g \frac{\partial^2 T_g}{\partial y^2} + h_{g,amb}\left(T_{amb} - T_g\right) + F_{g,sky} h_{g,sky}\left(T_{sky} - T_g\right) + F_{g,grd} h_{g,grd}\left(T_{grd} - T_g\right) + h_{g,abs}\left(T_{abs} - T_g\right) + \alpha_g G \tag{3}$$

where ρ_g denotes the density of the glass cover; δ_g is the thickness of the glass cover; c_g is the specific heat capacity of the glass cover at constant pressure; and λ_g is the thermal conductivity of the glass cover. T_g, T_{abs}, T_{amb}, T_{sky} and T_{grd} represent the temperatures of the glass cover, the PV absorber plate, the ambient air, the equivalent sky, and the ground, respectively. $F_{g,sky}$ and $F_{g,grd}$ are the view factors between the glass cover and the sky and the ground, respectively, for a vertical façade, both are taken as 0.5. α_g is the solar absorptance of the glass cover, and G is the solar irradiance.

For the PV absorber plate:

$$\rho_{abs}\delta_{abs}c_{abs}\frac{\partial T_{abs}}{\partial t} = \lambda_{abs}\delta_{abs}\frac{\partial^2 T_g}{\partial y^2} + h_{g,abs}\left(T_g - T_{abs}\right) + h_{abs,air}\left(T_{air} - T_{abs}\right) + h_{abs,back}\left(T_{back} - T_{abs}\right) + \tau_g \alpha_{abs} G - \xi E''_{PV} \tag{4}$$

where τ_g is the transmittance of the glass cover to solar radiation; α_{abs} is the solar absorptance of the PV absorber plate; ξ is the coverage ratio of the PV cells, defined as the ratio of the PV cell area to the absorber plate area; E''_{PV} is the electrical power generated by the photovoltaic cells per unit area, which can be calculated using a simple efficiency model as follows (Yu et al., 2022):

$$E''_{PV} = G\tau_g \eta_{ref}\left[1 - Br\left(T_{abs} - T_{ref}\right)\right] \tag{5}$$

In addition, $h_{abs,back}$ and $h_{abs,air}$ denote the radiative heat transfer coefficient between the PV absorber plate and the back plate, and the convective heat transfer coefficient between the PV absorber plate and the air in the flow channel, respectively.

$$h_{abs,back} = \frac{\sigma\left(T_{abs}^2 + T_{back}^2\right)(T_{abs} - T_{back})}{1/\varepsilon_{abs} + 1/\varepsilon_{back} - 1} \tag{6}$$

$$h_{abs,air} = \frac{Nu_{abs,air}\lambda_{air}}{H_{duct}} \tag{7}$$

where ε_{abs} and ε_{back} are the emissivities of the rear surface of the PV absorber plate and the back plate, respectively; H_{duct} is the height of the PV absorber plate, $Nu_{abs,air}$ is the Nusselt number for convective heat transfer between the PV absorber plate and the air in the flow channel (Smolec and Thomas, 1993).

$$Nu_{abs,air} = 0.12\left(Gr_{abs,air}Pr\right)^{1/3} \tag{8}$$

The air inside the flow channel primarily undergoes convective heat transfer with the PV absorber plate and the back plate; therefore, its energy conservation equation can be written as:

$$\rho_{air}c_{air}\delta_{duct}\frac{\partial T_{air}}{\partial t} = -\rho_{air}c_{air}u_{air}\delta_{duct}\frac{\partial T_{air}}{\partial y} + h_{abs,air}(T_{abs} - T_{air}) + h_{air,back}(T_{back} - T_{air}) \tag{9}$$

where δ_{duct} is the thickness of the air flow channel; $h_{air,back}$ is the convective heat transfer coefficient between the air in the flow channel and the back plate; u_{air} is the air velocity in the flow channel, which can be determined from the force balance between buoyancy and flow resistance acting on the air within the channel.

$$u_{air} = \sqrt{\frac{g\beta(T_{out} - T_{in})H_{duct}}{c_f\frac{H_{duct}}{d_{h,duct}} + c_{in}\left(\frac{A_{duct}}{A_{in}}\right)^2 + c_{out}\left(\frac{A_{duct}}{A_{out}}\right)^2 + c_{damper}\left[\left(\frac{A_{duct}}{A_{in}}\right)^2 + \left(\frac{A_{duct}}{A_{in}}\right)^2\right]}} \tag{10}$$

where T_{in} and T_{out} are the air temperatures at the inlet and outlet of the flow channel, respectively. Aduct, A_{in}, A_{out} are the cross-sectional area of the flow channel, the inlet area, and the outlet area, respectively. $d_{h,duct}$ is the hydraulic diameter of the flow channel. c_{in}, c_{out}, c_f and c_{damper} are the inlet local loss coefficient, outlet local loss coefficient, friction loss coefficient along the flow path, and the local loss coefficient of the damper, respectively (Sun et al., 2011, Smolec and Thomas, 1993, Gan and Riffat, 1999).

The energy conservation of the back plate mainly involves radiative heat transfer with the PV absorber plate, convective heat transfer with the air in the flow channel, and heat conduction through the insulation layer to the wall.

$$\rho_{back}c_{back}\delta_{back}\frac{\partial T_{back}}{\partial t} = \lambda_{back}\delta_{back}\frac{\partial^2 T_{back}}{\partial y^2} + h_{abs,back}(T_{abs} - T_{back}) + h_{air,back}(T_{air} - T_{back}) + \lambda_{back}\frac{T_{wall,ex} - T_{back}}{\delta_{ins}} \tag{11}$$

where λ_{ins} is the thermal conductivity of the insulation material; δ_{ins} is the thickness of the insulation material; $T_{wall,ex}$ is the temperature of the exterior surface of the wall.

For the wall serving as the building envelope, only heat conduction in the thickness direction is considered;

therefore, its energy conservation equation can be written as:

$$\rho_{wall} c_{wall} \frac{\partial T_{wall}}{\partial t} = \lambda_{wall} \frac{\partial^2 T_{wall}}{\partial x^2} \tag{12}$$

The boundary condition at the exterior surface of the wall can be written as:

$$-\lambda_{wall} \frac{\partial T_{wall}}{\partial x}\Big|_{x=0} = \lambda_{ins} \frac{T_{back} - T_{wall,ex}}{\delta_{ins}} \tag{13}$$

$$-\lambda_{wall} \frac{\partial T_{wall}}{\partial x}\Big|_{x=0} = h_{wall,amb}\left(T_{amb} - T_{wall,ex}\right) + F_{wall,sky} h_{wall,sky}\left(T_{sky} - T_{wall,ex}\right) + F_{wall,grd} h_{wall,grd}\left(T_{grd} - T_{wall,ex}\right) + \alpha_g G \tag{14}$$

For the bioaerosols within an infinitesimal control volume in the flow channel, the increase in the number of bacterial aerosols per unit time is balanced by the bacterial aerosols entering and leaving the control volume through the upstream and downstream boundaries, as well as those inactivated within the control volume. Accordingly, the governing equation can be written as:

$$W_{duct} \delta_{duct} dy \frac{\partial C}{\partial t} = WC(y) - QC(y + dy) - rW_{duct} \delta_{duct} dy \tag{15}$$

where W_{duct}, δ_{duct} and d are the width, thickness, and height of the infinitesimal control volume in the flow channel; Q is the volumetric airflow rate in the channel, which can be calculated from the channel cross-sectional area and the air velocity and r is the inactivation rate of bioaerosols per unit volume. If a first-order kinetic model is adopted, r is proportional to the bioaerosol concentration C and and the inactivation rate constant k. Accordingly, by slightly rearranging the above equation, one obtains:

$$\frac{dC}{dt} = -V_{air} \frac{\partial C}{\partial y} - kC \tag{16}$$

The dependence of the inactivation rate constant on temperature is described by the Arrhenius equation.

The system model is mainly solved using the finite difference method, in which the above heat and mass transfer equations are fully discretized in an implicit manner. The conduction terms are discretized using a second-order central difference scheme, while the convection terms are treated with a first-order upwind scheme. A numerical code is then developed to solve the resulting system of discretized equations using iterative methods such as the Jacobi or Gauss-Seidel algorithms, thereby obtaining the thermal and electrical outputs of the system as well as the evolution of bacterial aerosol concentration under different operating conditions. The overall simulation workflow is illustrated in Fig. 2(b).

This approach enables rapid prediction of the overall system behavior with high computational efficiency; however, it relies on empirical correlations and has limited capability in resolving the spatial non-uniformity of the flow and temperature fields. Moreover, this method is not well suited for quantitatively capturing the deposition behavior of bioaerosols within the flow channel.

3.3. SPATIALLY RESOLVED HIGH-DIMENSIONAL MODEL

High-dimensional numerical models based on spatially resolved solutions can simultaneously resolve the airflow organization, temperature distribution, particle transport, and local residence-time characteristics within the flow channels of the building envelope. The typical modeling procedure can be divided into the following four steps:

1. Establish the computational domain based on the physical configuration of the building envelope and generate the computational mesh.

2. The air flow and heat transfer processes are described using the conservation equations of mass, momentum, and energy. Turbulence effects are closed by selecting an appropriate Reynolds-averaged Navier-Stokes (RANS) model according to the Reynolds number and flow characteristics. Radiative heat transfer is accounted for by introducing a radiation transport model and coupling it as a radiative source term in the energy equation. The continuity, momentum, and energy equations adopted under steady-state conditions are given below, in which the turbulence terms are treated using the RNG k-ε model (Wu et al., 2022, Abdeen et al., 2019), and the radiation term is described using the DO model.

Continuity equation:

$$\frac{\partial C}{\partial x_i}(\rho u_i) = 0 \tag{17}$$

Conservation of momentum equation:

$$\frac{\partial}{\partial x_j}\left(\rho u_i u_j\right) = -\frac{\partial p}{\partial x_i} + \frac{\partial}{\partial x_j}\left(\mu \frac{\partial u_i}{\partial x_j} - \rho\overline{u_i' u_j'}\right) + S_i \tag{18}$$

Conservation of energy equation in fluid domain:

$$\frac{\partial(\rho u_i T)}{\partial x_i} = \frac{\partial}{\partial x_i}\left[\left(\frac{\mu}{Pr} + \frac{\mu_t}{\sigma_t}\right)\frac{\partial T}{\partial x_i} - \rho\overline{u_i' T'}\right] + S \tag{19}$$

Discrete coordinate radiation model:

$$\nabla(I(\vec{r},\vec{s})\vec{s}) + (\alpha + \sigma_s)I(\vec{r},\vec{s}) = \alpha n^2 \frac{\sigma T^4}{\pi} + \frac{\sigma_s}{4\pi}\int_0^{4\pi} I\left(\vec{r},\vec{s'}\right)\Phi\left(\vec{s},\vec{s'}\right)\, d\Omega' \tag{20}$$

3. The transport and evolution of bioaerosols can be described using different modeling frameworks, mainly including the Eulerian approach based on the continuous medium assumption (concentration transport equation) and the Lagrangian approach based on particle trajectory tracking (discrete phase model, DPM). The two bioaerosol modeling approaches are introduced separately in the following sections.

In the Eulerian approach, bioaerosols are treated as a continuous phase, and their transport is governed by a convection-diffusion equation. Considering the effect of gravity on bioaerosol transport, a drift velocity is introduced to modify the convective term, which can be expressed as:

$$\frac{\partial C}{\partial t} + \nabla \cdot [(V + V_s)C] = \nabla \cdot \left[\left(\varepsilon_p + D\right)\nabla C\right] + S \tag{21}$$

where V is the airflow velocity field; V_s is gravity settling velocity field; ε_p is particle turbulent diffusion coefficient; D is particle Brownian diffusion coefficient and S is the source term for inactivation of infectious bioaerosols due to high temperature, which is calculated as:

$$\mathrm{S} = -\mathrm{kC} = -\mathrm{A}e^{-\frac{Ea}{RT}}\mathrm{C} \tag{22}$$

For bioaerosol deposition on solid surfaces, the particle deposition flux at the wall can be described based on a modified form of Fick's law (Zhao and Chen, 2006):

$$\mathrm{J} = -\left(\varepsilon_p + \mathrm{D}\right)\frac{\partial C}{\partial n} + V_s \mathrm{C} cos\theta + \bar{V}_{pn}^{c}\mathrm{C} \tag{23}$$

where J is particle deposition flux to the wall. V_s is particle gravity settling velocity and is particle convection velocity in the direction $\vec{n}$, which describes gravity mechanism and inertia mechanism, respectively. Moreover, θ is defined by the angle between the wall-normal and vertical directions, as shown in Fig. 2(c).

The particle Brownian diffusion coefficient is given by the Stocks-Einstein formula:

$$D = \frac{kT}{3\pi\mu d_p} \tag{24}$$

where K = 1.38×10-16 J/K is Boltzmann constant, μ is viscosity of the medium, d_p is the diameter of particle.

The particle turbulent diffusion coefficient is given by the semi-empirical equation:

$$\varepsilon_p = \mu_t \left(1 + \frac{\tau_p}{T_l}\right)^{-1} \tag{25}$$

where μ_t is turbulent viscosity of turbulent flow, τ_p is particle relaxation time, which is calculated as $\tau_p = \frac{C_p \rho_p d_p}{18\mu}$, T_l is Lagrangian time scale of fluid turbulence, which is calculated as $T_l = \frac{\mu_t}{\overline{V_{fn}'^2}}$.

By establishing a force balance among gravity, drag, and buoyancy acting on particles suspended in air, the particle gravitational settling velocity can be obtained as:

$$V_s = \frac{C_c g d_p^2 \left(\rho_p - \rho\right)}{18\mu} \tag{26}$$

Where ρ is density of the medium, C_c is the Cunningham coefficient, which is a revision for fine particles (d_p < 10 μm) and can be calculated as:

$$C_c = 1 + \frac{\lambda}{d_p}\left(2.514 + 0.8\exp\left(-0.55\frac{d_p}{2\lambda}\right)\right) \tag{27}$$

Where λ is the mean free length of the air molecule.

Following Guha's report (Guha, 2008), the particle convection velocity can be constructed from gradients in turbulence intensity and expressed as:

$$\bar{V}_{pn}^{c} = -\tau_p \frac{d}{dy}\left(\overline{V_{py}'^2}\right) \tag{28}$$

Where $\left(\overline{V_{pn}'^2}\right)$is the particle mean square velocity, based on the simple theories of homogeneous, isotropic turbulence (Reeks, 1977), particle mean square velocity can be expressed as:

$$\overline{V_{pn}'^2} = \overline{V_{fn}'^2}\left(\frac{T_L}{\tau_p + T_L}\right) \tag{29}$$

To simplify the form particle deposition flux to the wall, the deposition velocity is defined as:

$$V_d = \frac{|J(y=0)|}{C_\infty} \tag{30}$$

Where C_∞ is particle concentration outside the boundary layer. The dimensionless deposition velocity can be written as:

$$V_d^+ = \left(\frac{D+\varepsilon_p}{v_t}\right)\frac{\partial C^+}{\partial y^+} + V_s^+ C^+ \cos\theta + \bar{V}_{pn}^{c+} C^+ \tag{31}$$

Where $V_d^+, V_s^+, \bar{V}_{pn}^{c+}$ are results normalized by friction velocity u^*; C^+ is the result normalized by C_∞.

In the Lagrangian framework, airborne bioaerosols are treated as discrete particles, and their transport and evolution are described by tracking the trajectories of individual particles within the resolved airflow and temperature fields. The gas-phase flow and heat transfer processes are solved using the Eulerian approach, while the particle phase is computed based on the known gas-phase velocity and temperature fields under a one-way coupling assumption.

The motion of an individual bioaerosol particle follows Newton's second law, and its velocity evolution equation can be written as (Lu and Lu, 2015):

$$\frac{du_p}{d_t} = F_D(u-u_p) + g\frac{\rho_p-\rho}{\rho_p} + F_{lift} + F_{therm} \tag{32}$$

where u_p and u denote the particle velocity and the gas-phase velocity, respectively, while ρ_p and ρ represent the densities of the particle and air. The terms on the right-hand side correspond to the aerodynamic drag force, gravity with buoyancy correction, shear-induced lift force, and the thermophoretic force arising from temperature gradients, respectively. For micrometer-scale bioaerosols, the aerodynamic drag force is the dominant term, which can be expressed as:

$$F_D = \frac{18\mu}{\rho_p d_p^2}\frac{C_D Re_p}{24} \tag{33}$$

where μ is the dynamic viscosity of air and d_p is the particle diameter.

The interaction between bioaerosols and solid surfaces is described through wall boundary conditions. For the PV absorber plate, back plate, and other solid walls within the flow channel, a "trap" boundary condition is applied: when a particle trajectory comes into contact with a wall, the particle is assumed to deposit and is removed from the computational domain (Liu et al., 2023a). By statistically analyzing particle capture events on different surfaces, the spatial distribution of bioaerosol deposition and the corresponding deposition flux can be obtained.

Based on the above particle deposition modeling results, it can be observed that particle deposition behavior exhibits a unified dependence on the dimensionless particle relaxation time, regardless of the numerical framework employed (Fig. 2(d)). Specifically, when the particle relaxation time is small (St << 1), particles respond rapidly to turbulent fluctuations, and the deposition process is dominated by turbulent diffusion and molecular diffusion, resulting in relatively low deposition velocities. As the relaxation time increases to an intermediate range (St ≈ 1), particle inertia becomes increasingly important, and the combined effects of eddy diffusion and inertial impaction lead to a rapid increase in deposition velocity. With a further increase in relaxation time (St >> 1), particle motion gradually decouples from turbulent fluctuations, and the deposition process becomes inertia-modulated, with the growth rate of deposition velocity tending to level off (Tian and Ahmadi, 2007, Liu and Agarwal, 1974, El-Shobokshy, 1983, Friedlander and Johnstone, 1957, Li and Ahmadi, 1993, Qian et al., 2024c). Notably, this three-regime deposition behavior can be captured not only by Lagrangian particle tracking approaches but also by Eulerian-based particle transport and deposition models, indicating a consistent representation of the underlying deposition mechanisms across different modeling frameworks.

For bioaerosols inactivation, the survival probability relative to the initial number can be expressed as:

$$\frac{N_t}{N_0} = exp(-kt) \tag{34}$$

In Lagrangian particle tracking, greater emphasis is placed on the instantaneous survival probability between two successive time steps, denoted as $P_{survival}(t)$, which is defined as:

$$P_{survival}(t) = exp(-k\Delta t) \tag{35}$$

At each time step, a random number ζ uniformly distributed between 0 and 1 is generated for each bioaerosol particle, and its state is determined according to the following criterion. When a sufficiently large number of particles is tracked, the statistical uncertainty introduced by the random process can be neglected (Pan et al., 2023).

$$\begin{cases} \zeta < P_{survival}(t), active \\ \zeta \geq P_{survival}(t), inactive \end{cases} \tag{36}$$

4. Boundary conditions are applied at the inlet, outlet, and walls, such as volumetric flow rate or velocity inlet, pressure outlet, wall temperature or heat flux, and equivalent heat sources induced by solar irradiation, while necessary thermal boundary conditions, including heat conduction, convective heat transfer, and radiative heat transfer, are also taken into account.

Although this methods offer clear advantages in resolving complex coupled processes in detail, they are associated with high computational cost and significant uncertainties arising from multiple parameters, which limit their direct application to system-level optimization and long-term operational analysis. Therefore, achieving a balance between computational efficiency and physical fidelity, and developing a multi-level modeling and solution framework suitable for analyzing the coupled optical-electrical-thermal-purification behavior of building envelopes, remains an important research direction that warrants further investigation in this field.

Low-dimensional numerical models based on streamwise discretization are usually implemented in in-house codes and validated against system-level measurements (e.g., outlet air temperature, thermal/electrical outputs, and overall purification/inactivation efficiency), most often using in-house experimental data and occasionally public datasets. By contrast, high-dimensional spatially resolved models are typically built on CFD platforms (e.g., Fluent or OpenFOAM); they generally require mesh/time-step verification and are then validated against the same system-level metrics. Computationally, low-dimensional models run fast and are suitable for large parametric sweeps and iterative optimization, whereas CFD is far more expensive and strongly dependent on mesh resolution (and time-step settings).

For coupled thermal–bioaerosol simulations, the main uncertainties come from:

1. Time-varying operating and environmental conditions (solar irradiance, indoor/outdoor temperature, wind speed), which reshape residence time and thermal exposure, and
2. assumptions in particle transport/deposition, especially whether humidity/UV/combined effects are included and how particle size is specified (single size vs. distribution). These choices can materially shift predicted purification and inactivation performance.

Taken together, these modeling frameworks provide the necessary input-output mapping between design/operation variables and system-level performance, thereby forming the basis for subsequent optimization aimed at balancing energy outputs and indoor air-quality targets.

4. SYSTEM OPTIMIZATION

Based on the studies of Xie et al. (Xie et al., 2024b) and Meng et al. (Meng et al., 2025), it can be concluded that there remains considerable room for improvement in the air-purification performance of conventional self-powered, self-purifying building envelope systems. Specifically, owing to the higher thermal resistance of Gram-positive bacteria, the removal efficiency of bioaerosols containing Gram-positive species is relatively limited. Moreover, under low solar irradiance conditions, the temperature within the building envelope is

insufficient to effectively inactivate bioaerosols within short exposure times.

In view of the above limitations, this section builds upon the previously established coupled light-electrical-thermal-purification model and introduces system optimization theories and methods. From the perspectives of structural optimization and operational optimization, effective approaches are systematically explored to enhance the overall performance of self-powered, self-purifying building envelopes, with particular emphasis on improving air-purification performance.

4.1. STRUCTURE-LEVEL OPTIMIZATION

To enhance the air-purification performance of the system, two main approaches can be considered: strengthening thermal inactivation and introducing additional inactivation mechanisms. According to the experimental results reported by Xie et al. (Wang et al., 2019), increasing the exposure temperature of bioaerosols and prolonging their residence time under high-temperature conditions can significantly improve their inactivation efficiency.

4.1.1. STRENGTHENING THERMAL INACTIVATION

Based on the above principles, Qian et al. (Qian et al., 2024c, Qian et al., 2024a) proposed a self-powered, self-purifying building envelope incorporating a finned structure, as schematically illustrated in Fig. 3(a). Compared with the conventional configuration, the primary modification of this system lies in the design of the absorber: a series of transverse fins are welded to the rear side of the absorber. The introduction of fins significantly increases the effective heat-transfer area between the airflow and the absorber, thereby enhancing heat transfer and enabling the air passing through the system to reach higher temperatures. Meanwhile, the finned structure prolongs the residence time of the airflow within the channel, which is beneficial for improving air-purification performance.

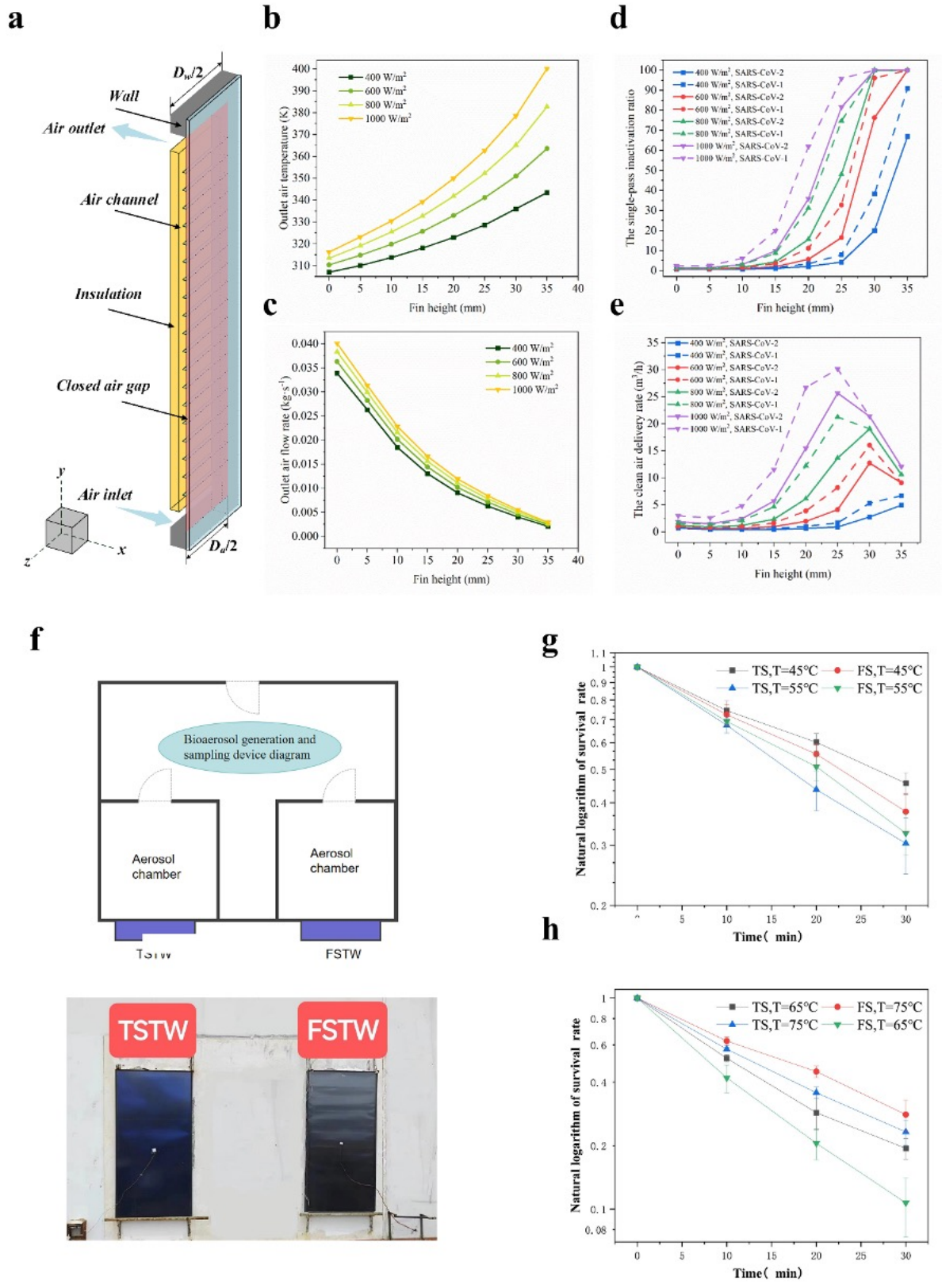

Figure 3. Self-powered and self-purifying building envelope with finned structures. **(a)** Schematic of the building envelope configuration; **(b)** Variation of outlet air temperature with fin height; **(c)** Variation of outlet air flow rate with fin height; **(d)** Variation of single-pass removal efficiency with fin height; **(e)** Variation of clean air delivery rate with fin height; **(f)** Experimental setups of the two building envelope configurations; **(g)** Removal performance of indoor bioaerosols by the two envelopes at 45 °C and 55 °C; **(h)** Removal performance of indoor bioaerosols by the two envelopes at 65 °C and 75 °C.

Numerical simulation results indicate that as the fin height increases from 0 mm to 35 mm, the outlet air temperature rises markedly, as shown in Fig. 3(b). Meanwhile, the ventilation rate decreases due to the

reduction in the free-flow cross-sectional area for airflow (Fig. 3(c)). Benefiting from the elevated air temperature and extended residence time, the single-pass inactivation efficiency of infectious bioaerosols increases significantly with fin height (Fig. 3(d)). However, because the clean air delivery rate is jointly affected by both the single-pass inactivation efficiency and the ventilation rate, a trade-off exists between these two factors, resulting in a non-monotonic variation of the clean air delivery rate with fin height, as illustrated in Fig. 3(e).

The calculation methods for the single-pass inactivation efficiency and the clean air delivery rate are given as follows. The single-pass inactivation ratio is calculated by:

$$\varepsilon_v = \frac{C_{in} - C_{out}}{C_{in}} \times 100\% \tag{43}$$

where C_{in} and C_{out} are inlet and outlet infectious bioaerosol concentration. Clean air delivery rate (CADR) indicates the amount of purified air per unit time which is presented as follows:

$$CADR = Q\varepsilon_v \tag{44}$$

Meng et al. (Meng et al., 2025) further constructed experimental chambers equipped with a conventional self-powered, self-purifying Trombe wall (TSTW) and a finned self-powered, self-purifying Trombe wall (FSTW), as shown in Fig. 3(f), and comparatively investigated the removal performance of indoor infectious bioaerosols under different temperature conditions (Fig. 3(g-h)). Under low-temperature conditions (45°C), the FSTW system exhibited superior indoor disinfection performance compared with the conventional TSTW system, owing to its ability to increase air temperature and prolong residence time. As the operating temperature increased to the intermediate range (55°C), differences in ventilation flow rates between the two systems became increasingly pronounced, with the TSTW system delivering a substantially larger amount of exchange air than the FSTW system. Benefiting from the higher airflow rate, the advantage of the TSTW system accumulated over time, leading to a gradual reversal in which its overall indoor disinfection performance surpassed that of the FSTW system. At higher temperature conditions (65°C and 75°C), the TSTW system consistently outperformed the FSTW system in terms of indoor disinfection efficiency.

In addition to the finned configuration, Qian et al. (Qian et al., 2024b) proposed a series-connected self-powered, self-purifying building envelope, as schematically illustrated in Fig. 4(a). By connecting two stages in series, this configuration further increases the outlet air temperature and extends the residence time of infectious bioaerosols under high-temperature conditions, thereby significantly enhancing air-purification performance while maintaining relatively high electrical and thermal outputs. The results demonstrated that the series-connected system exhibits a clear advantage in air-purification capability compared with the conventional structure (Fig. 4(c-d)).

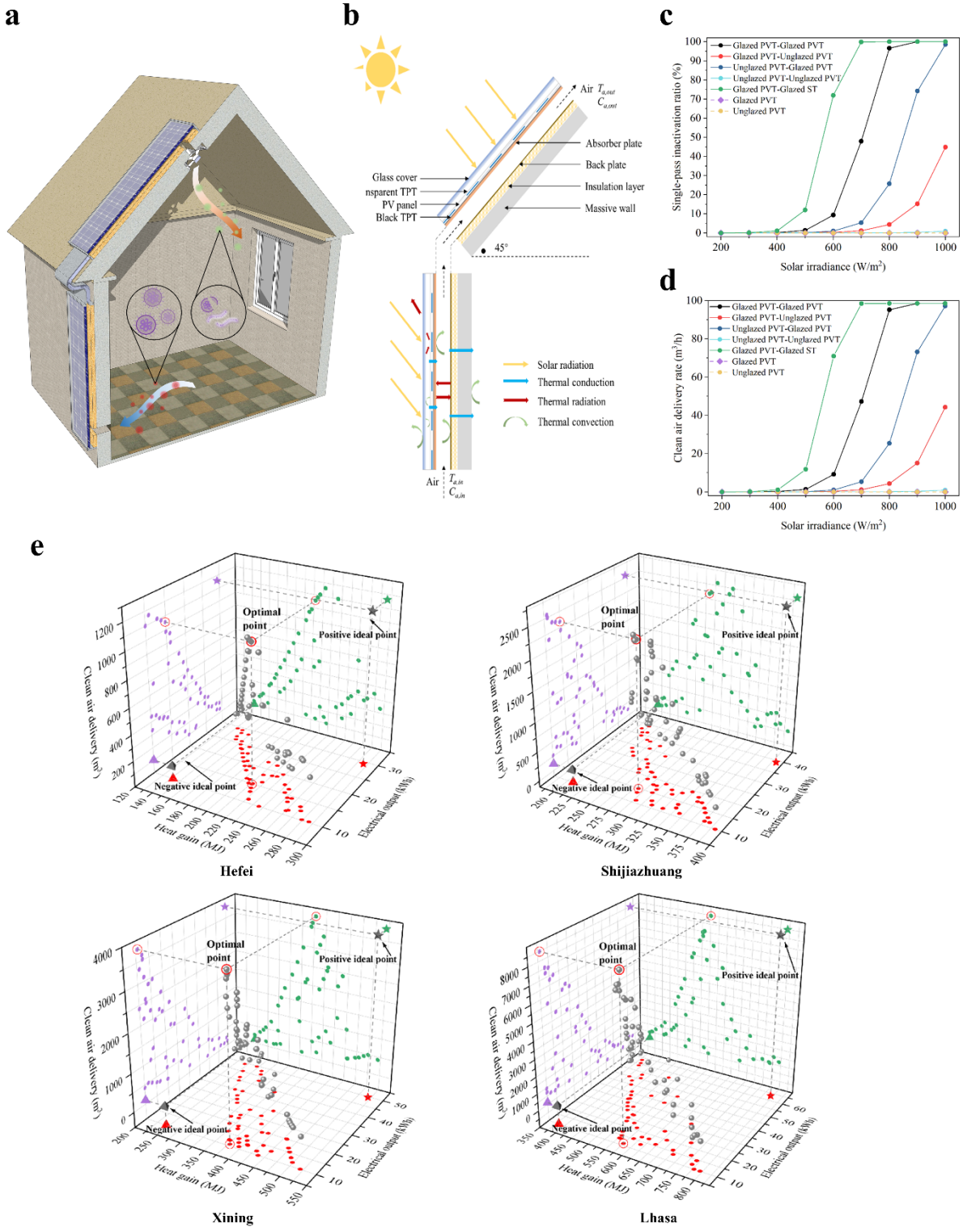

Figure 4. Series-type self-powered and self-purifying building envelope. **(a)** Schematic of a building integrated with the envelope system; **(b)** Schematic of the series-type envelope configuration; **(c)** Single-pass removal efficiency under different two-stage configurations; **(d)** Clean air delivery rate under different two-stage configurations; **(e)** Pareto fronts obtained from multi-objective optimization for four representative climate.

On this basis, the authors further pointed out that strong coupling and trade-offs exist among heating, power generation, and air-purification performance, making it difficult for single-objective-oriented designs to achieve optimal overall system performance. To address this issue, Qian et al. (Qian et al., 2024b) developed a multi-objective optimization framework for the series-connected system and conducted system-level optimization analyses under different climatic conditions, as shown in Fig. 4(e).

4.1.2. INTRODUCING ADDITIONAL INACTIVATION MECHANISMS

Xie et al. (Xie et al., 2024b) introduced filtration into self-powered, self-purifying building envelopes and proposed a novel photovoltaic-Trombe wall air filtration and disinfection system integrating power generation, air heating, and air purification. The incorporation of the filtration unit enables the capture of bacteria that survive within the airflow channel, while the continuous exposure of the filter to heated air effectively suppresses bacterial growth and proliferation on the filter surface. The results demonstrated that the system can achieve a sustained reduction in indoor bioaerosol concentrations throughout the day, as shown in Fig. 5(b).

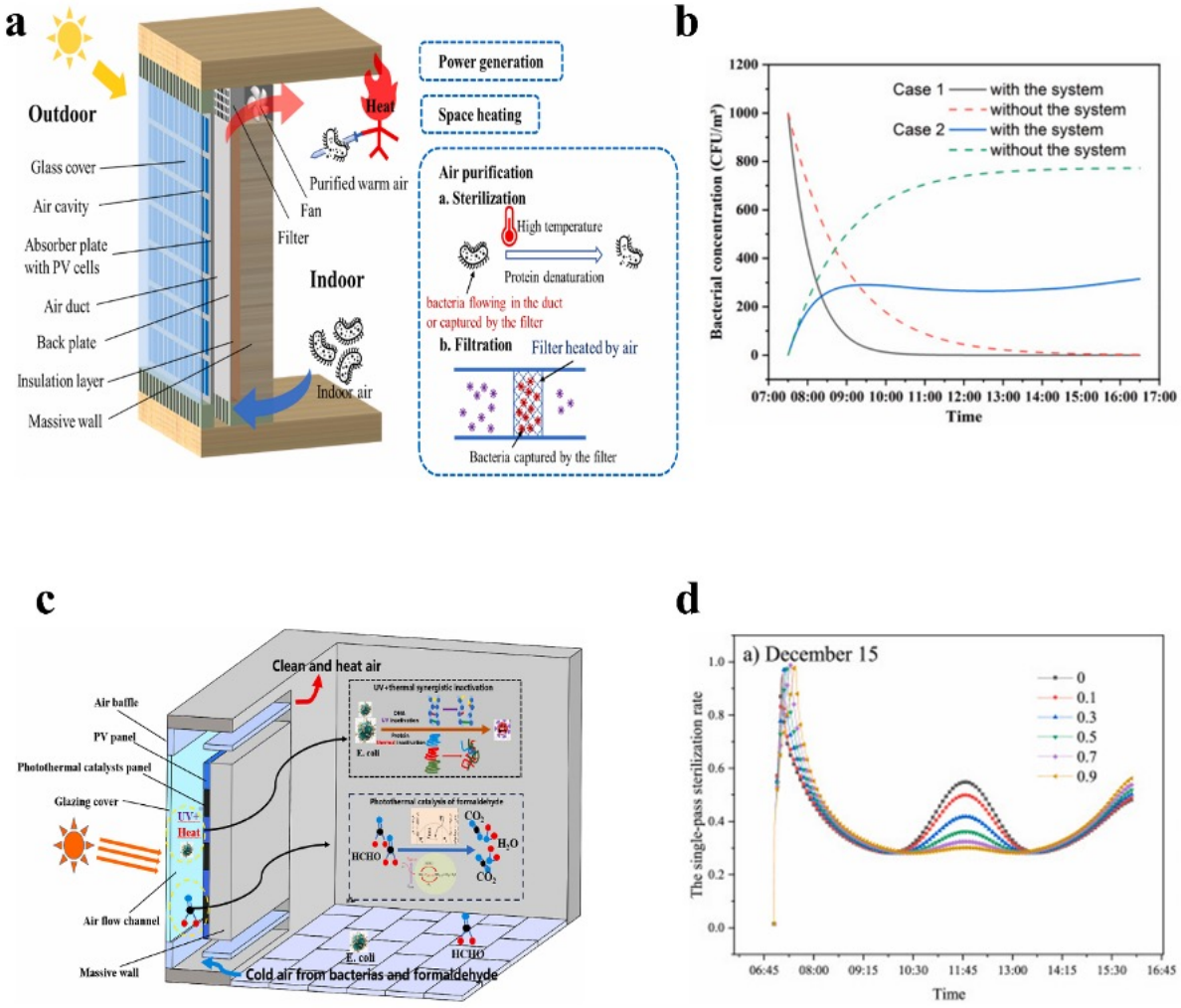

Figure 5. Self-powered and self-purifying building envelope incorporating different inactivation mechanisms. **(a)** Schematic of the envelope configuration with an outlet filter; **(b)** All-day indoor bacterial removal performance of the system; **(c)** Schematic of the envelope configuration incorporating ultraviolet inactivation; **(d)** All-day variation of single-pass removal efficiency.

Che et al. (Che et al., 2024) incorporated ultraviolet (UV) irradiation and thermal inactivation mechanisms into the building envelope by placing the absorber on the inner side of the airflow channel, allowing external UV radiation to penetrate through the glazing. As a result, bacteria in indoor air are inactivated through the combined effects of elevated temperature and UV exposure. The results revealed a typical three-stage diurnal inactivation pattern of indoor bacteria. In the initial stage, due to relatively low air temperature and velocity, the longer residence time allows UV inactivation to dominate. In the second stage, once the air temperature reaches the thermal inactivation threshold of bacteria, thermal inactivation becomes effective in removing most bacteria even under shortened residence times. In the third stage, as solar irradiance weakens and temperature decreases, the contribution of thermal inactivation gradually diminishes, and UV inactivation again becomes the dominant mechanism (see Fig. 5(d)).

Although these studies have demonstrated the potential to enhance the air-purification performance of self-

powered, self-purifying building envelopes, their application scenarios remain relatively limited. Existing investigations have mainly focused on low-rise buildings, with envelope systems typically configured as modular units of approximately 2m × 1m. Future studies should therefore explore the applicability of such systems across different climatic regions and building types, systematically evaluating the coupled light-electrical-thermal-purification performance under diverse operating conditions, and further elucidating their regional suitability and synergistic optimization mechanisms.

4.2. OPERATION-LEVEL OPTIMIZATION

In addition to structural optimization, the performance of self-powered, self-purifying building envelopes can be further enhanced through operation-level optimization. This study investigates two operation-level optimization strategies: day-ahead optimization and intra-day optimization. Day-ahead optimization focuses on planning system operation based on forecasted boundary conditions, with the objective of achieving an optimal balance among heating supply, power generation, and air-purification performance over a full-day horizon. In contrast, intra-day optimization targets short-term system operation under time-varying conditions, aiming to dynamically adjust control variables to improve system responsiveness and performance stability within the day. By addressing different temporal characteristics and operational objectives, day-ahead and intra-day optimization provide two complementary approaches for enhancing the operational performance of self-powered, self-purifying building envelopes under practical operating conditions.

4.2.1. DAY-AHEAD OPTIMIZATION STRATEGY

Qian et al. (Qian et al., 2025b) proposed a dynamically adjustable air-purification-oriented BIPVT system (Fig. 6(a)), in which multiple air outlets enable flexible switching among air purification, natural ventilation, and nighttime exhaust modes, thereby balancing air-purification effectiveness and system energy consumption under varying environmental conditions.

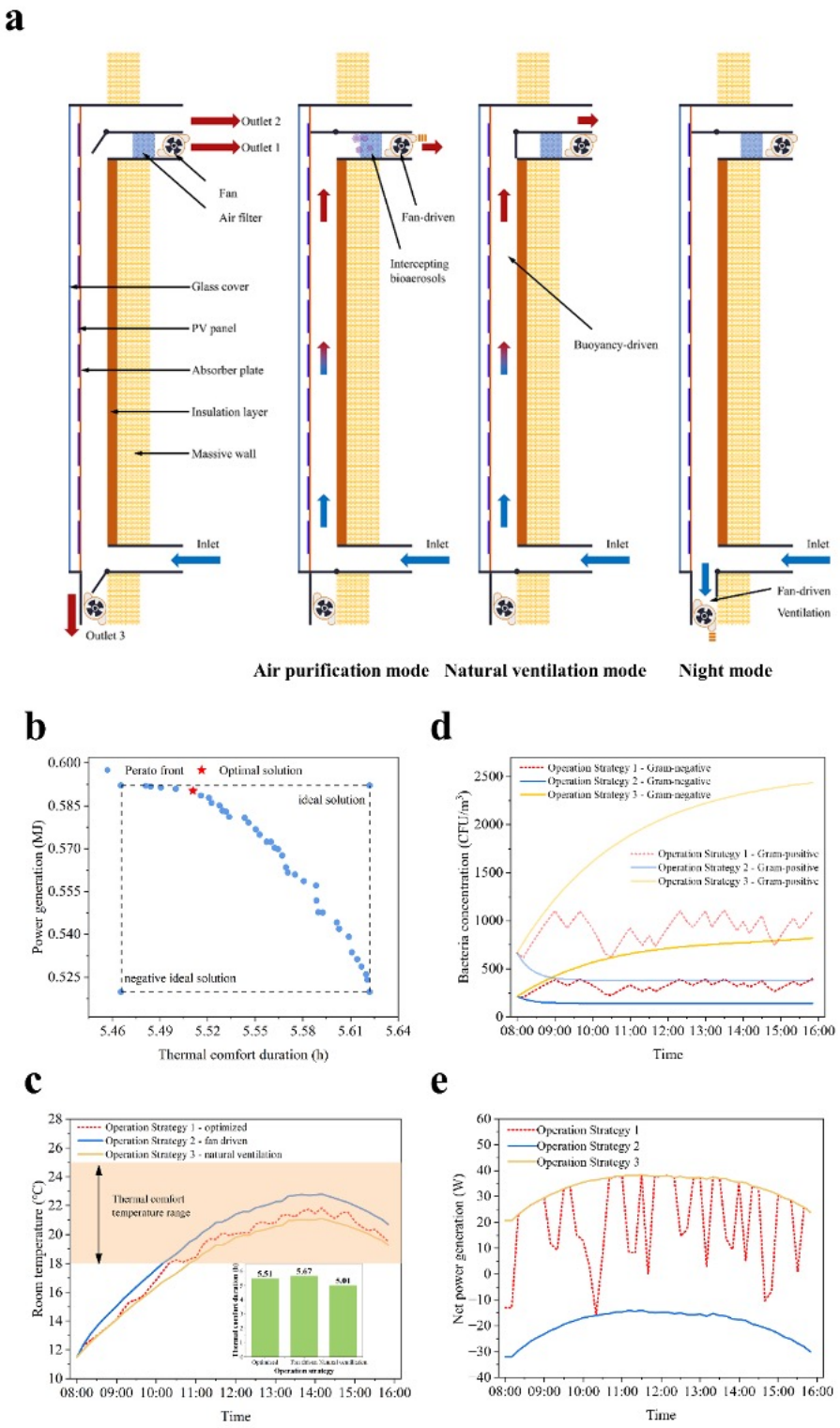

Figure 6. Day-ahead optimization strategy of the system. **(a)** Self-powered and self-purifying building envelope with dynamically adjustable capability; **(b)** Pareto front obtained from day-ahead multi-objective optimization; **(c)** Comparison of thermal performance between the optimized operational strategy and the static operation mode; **(d)** Comparison of air purification performance between the optimized operational strategy and the static operation mode; **(e)** Comparison of electrical performance between the optimized operational strategy and the static operation mode.

Based on this configuration, a dynamic operation optimization strategy was developed to periodically select the optimal operating mode and airflow rate. The optimization aims to maximize the duration of indoor thermal comfort (18-25°C) and electricity generation while satisfying the constraint that the indoor bacterial concentration remains below 1500 CFU m^3, in accordance with the Chinese Indoor Air Quality Standard (GB/T 18883-2022). Accordingly, the system operation problem is formulated as a multi-objective

optimization with thermal comfort duration and power generation as objectives and indoor air hygiene as a constraint. The resulting Pareto front is shown in Fig. 6(b). It should be noted that reported study adopts the Chinese indoor air quality standard as the evaluation criterion; however, international frameworks such as those proposed by the World Health Organization (WHO), ASHRAE, and European guidelines may adopt different indicators and threshold values for indoor air quality assessment .

Comparative results indicate that, compared with a conventional continuous fan operation strategy, the optimized dynamic strategy achieves a substantial energy-saving effect (208.5%) while maintaining indoor air quality safety with only a minor reduction in thermal comfort duration (0.16 h, 2.9%). In addition, relative to operation relying solely on natural ventilation, the optimized strategy significantly enhances air-purification performance, extending the duration during which indoor bacterial concentrations remain within the safe range by 7.16 h (Fig. 6(c-e)). These results demonstrate the considerable potential of operation-level dynamic optimization for enhancing the overall performance of air-purification-oriented BIPVT systems.

4.2.2. INTRA-DAY OPTIMIZATION STRATEGY

Considering uncertainties arising from weather forecast errors, occupant behavior, and variations in operating conditions, Qian et al. (Qian et al., 2025a) further proposed an intra-day rolling optimization strategy based on the aforementioned system. By dividing the scheduling horizon into multiple time intervals, this strategy continuously updates and adjusts system operation within a limited prediction window, enabling a rapid response to dynamic disturbances. The core idea is to make optimization decisions at each scheduling interval using the latest forecast information and to update the operating plan in a rolling manner, thereby balancing operational foresight and flexibility, with the overall objective of reducing energy costs while ensuring indoor thermal comfort and air quality. The corresponding optimization workflow is illustrated in Fig. 7(a).

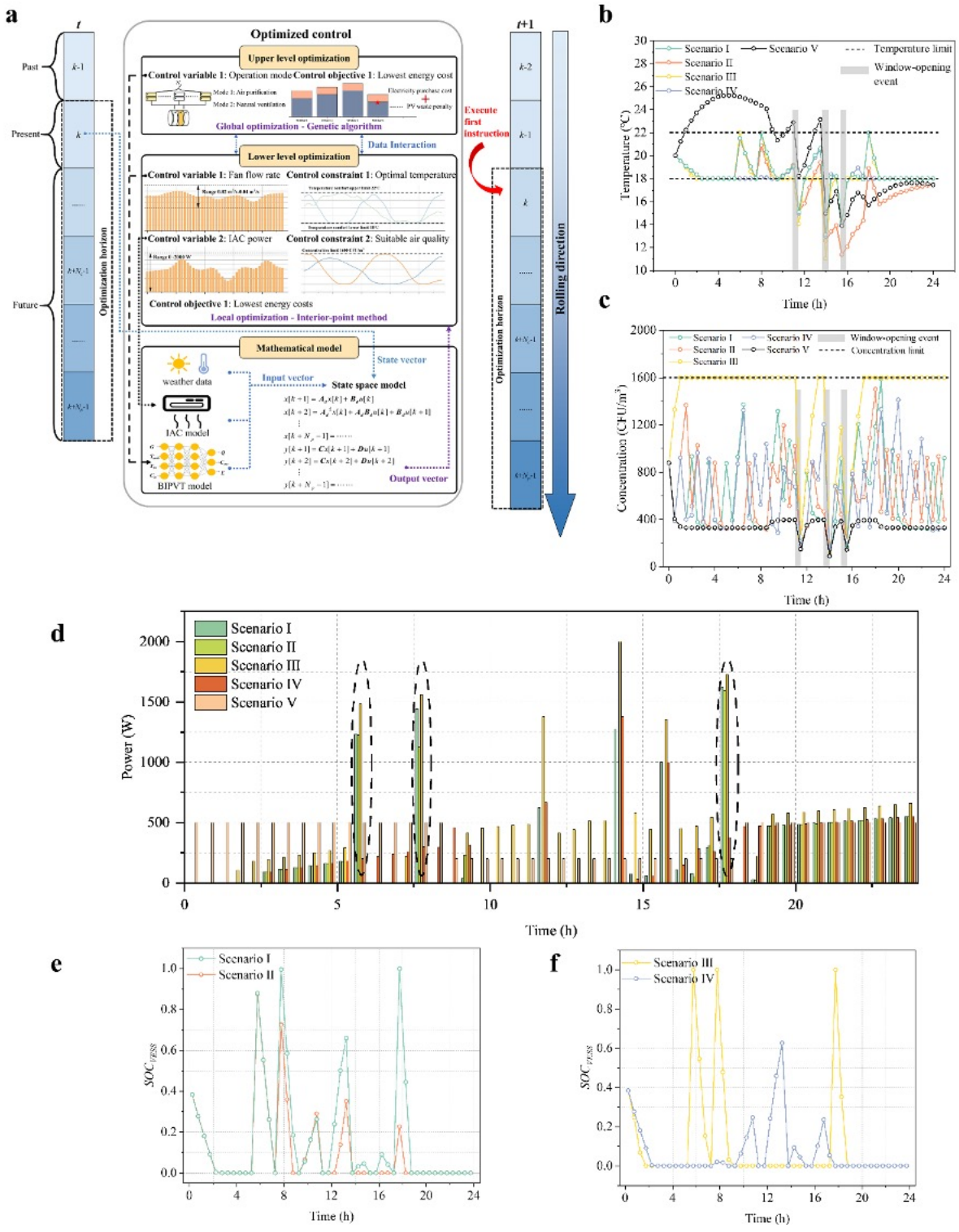

Figure 7. Intra-day optimization strategy of the system. **(a)** Workflow of the intra-day rolling optimization; **(b)** Comparison of thermal performance under different scenarios; **(c)** Comparison of air purification performance under different scenarios; **(d)** Comparison of electricity purchasing under different scenarios; **(e)** Building energy storage performance for Scenarios Ⅰ and Ⅱ; **(f)** Building energy storage performance for Scenarios Ⅲ and Ⅳ.

To evaluate the effectiveness of the proposed approach, the authors conducted a comparative analysis of thermal performance, power generation, indoor air quality, and energy costs across five different operating and control scenarios, including day-ahead optimization, intra-day rolling optimization, rule-based control, and various system configurations (Fig. 7(b-f)). The results demonstrate that, compared with the day-ahead optimization strategy, intra-day optimization exhibits a clear advantage in coping with unexpected disturbances. Under conditions involving weather forecast deviations and random window-opening events, the proposed intra-day optimization method reduces the thermal comfort violation rate by 78.9%.

Although existing studies have demonstrated the significant potential of operation-level optimization in enhancing system energy efficiency and air-purification performance, their application remains largely confined to single-room residential buildings, and integrated deployment and validation in real building environments are still lacking. Future work should therefore focus on system-level implementation and long-term operation in real buildings, and further assess the applicability and scalability of different optimization and control strategies in multi-room and large-scale commercial buildings.

An overview of system optimization approaches, key methods, and reported performance outcomes is summarized in Table 1.

Table 1. Overview of system optimization approaches, key methods, and reported performance outcomes.

Ref	Optimization level	Optimization objective	Optimization path	Optimization result
(Qian et al., 2024c, Qian et al., 2024a)	Structural	Improve air purification performance	Flow channel structure optimization	Single-pass inactivation ratio significantly increased
(Qian et al., 2024b)	Structural	Improve overall performance	Flow channel thickness and PV coverage optimization	Pareto front obtained for three-objective optimization
(Xie et al., 2024b)	Structural	Improve air purification performance	Filtration mechanism integration	Indoor bacterial concentration significantly reduced
(Che et al., 2024)	Structural	Improve air purification performance	UV disinfection mechanism integration	Air purification performance improved under low irradiance
(Qian et al., 2025b)	Operational	Maintain indoor thermal and air-quality conditions while reducing costs.	Day-ahead multi-objective optimization	Energy costs significantly reduced
(Qian et al., 2025a)	Operational	Maintain indoor thermal and air-quality conditions while reducing costs.	Intra-day bi-level rolling optimization	Energy costs significantly reduced

5. CONCLUSIONS AND PERSPECTIVES

Against the backdrop of increasingly stringent building energy conservation and carbon-reduction targets, together with growing concerns over indoor air pollution, the integration of solar energy utilization with reductions in building energy consumption and simultaneous improvements in indoor environmental quality has emerged as an important research direction. As a promising green building technology, solar-driven self-powered and self-purifying building envelopes have achieved notable progress in recent years, particularly in terms of mechanistic understanding, system modeling and optimization. Along this trajectory, existing studies have progressively elucidated the thermal inactivation behaviors of pathogenic microorganisms under short exposure times and non-isothermal conditions, developed coupled light-electrical-thermal-purification modeling and solution methods tailored to building envelopes, and preliminarily established multi-level system optimization frameworks aimed at enhancing air-purification performance.

Despite these advances, several challenges remain. Future research should focus on the following directions. First, inactivation models for bacteria and viruses under multi-parameter coupled conditions, including temperature, humidity, and ultraviolet irradiation, should be developed to more realistically capture microbial inactivation behaviors under practical operating conditions. Second, there is a need to advance multi-level modeling and solution frameworks that balance computational efficiency with physical fidelity, enabling effective analysis of the coupled light-electrical-thermal-purification processes in building envelopes at the system level. Finally, the applicability of such systems across different climatic regions and building types should be systematically explored, with comprehensive evaluations of their coupled performance under diverse operating conditions, and further elucidation of regional suitability as well as the synergistic mechanisms between system configuration and operational optimization.

AUTHOR CONTRIBUTIONS

Yu Qian: Conceptualization, Investigation, Visualization, Methodology, Software, Data curving, Validation, Writing-original draft. **Jie Ji**: Conceptualization, Supervision, Funding acquisition. **Suyue Xu**: Writing-original draft. **Yifei Gao**: Writing-original draft. **Ziheng Li**: Writing-original draft. **Hengmin Jia**: Investigation. **Yan Mu**: Investigation.

COMPETING INTERESTS

The authors declare that they have no known competing financial interests or personal relationships that could have appeared to influence the work reported in this paper.

DATA ACCESSIBILITY

Data will be available on request.

REFERENCES

Ashrae. Ansi/Ashrae Standard 62.2-2022: Ventilation and Acceptable Indoor Air Quality in Residential Buildings. ASHRAE, 2022.

European Commission. EN 16798-1: Energy Performance of Buildings—Ventilation for Buildings. CEN, 2019.

World Health Organization. WHO Global Air Quality Guidelines. WHO Press, 2021.

Abdeen, A., Serageldin, A. A., Ibrahim, M. G. E., El-Zafarany, A., Ookawara, S. & Murata, R. 2019. Experimental, analytical, and numerical investigation into the feasibility of integrating a passive Trombe wall into a single room. Applied Thermal Engineering, 154, 751-768. DOI: https://doi.org/10.1016/j.applthermaleng.2019.03.090.

Asaee, S. R., Nikoofard, S., Ugursal, V. I. & Beausoleil-Morrison, I. 2017. Techno-economic assessment of photovoltaic (PV) and building integrated photovoltaic/thermal (BIPV/T) system retrofits in the Canadian housing stock. Energy and Buildings, 152, 667-679. DOI: https://doi.org/10.1016/j.enbuild.2017.06.071.

Che, L., Li, N., Fan, M., Zhang, G., Zhang, G. & Yu, B. 2024. A novel catalytic/sterilization PV-Trombe wall system: Analysis on PV electrical and air purification performance in winter. Building and Environment, 255. DOI: https://doi.org/10.1016/j.buildenv.2024.111423.

Chow, T. T. 2018. A review on photovoltaic/thermal hybrid solar technology. Renewable Energy, Vol4_88-Vol4_119. DOI: https://doi.org/10.1016/j.apenergy.2009.06.037.

El-Shobokshy, M. 1983. Experimental measurements of aerosol deposition to smooth and rough surfaces. Atmospheric Environment (1967), 17, 639-644. DOI: https://doi.org/10.1016/0004-6981(83)90138-5.

Friedlander, S. & Johnstone, H. 1957. Deposition of suspended particles from turbulent gas streams. Industrial & Engineering Chemistry, 49, 1151-1156. DOI: https://pubs.acs.org/doi/10.1021/ie50571a039.

Gan, G. & Riffat, S. 1999. Determination of energy loss characteristics of dampers. International journal of energy research, 23, 61-69. DOI: https://doi.org/10.1002/(SICI)1099-114X(199901)23:1<61::AID-ER461>3.0.CO;2-S.

Guha, A. 2008. Transport and Deposition of Particles in Turbulent and Laminar Flow. Annual Review of Fluid Mechanics, 40, 311-341. DOI: https://doi.org/10.1146/annurev.fluid.40.111406.102220.

Herrando, M., Markides, C. N. & Hellgardt, K. 2014. A UK-based assessment of hybrid PV and solar-thermal systems for domestic heating and power: System performance. Applied Energy, 122, 288-309. DOI: https://doi.org/10.1016/j.apenergy.2014.01.061.

Jung, J. H., Lee, J. E. & Kim, S. S. 2009. Thermal effects on bacterial bioaerosols in continuous air flow. Sci Total Environ, 407, 4723-30. DOI: https://doi.org/10.1016/j.scitotenv.2009.05.008.

Ke, W., Ji, J., Xu, L., Xie, H., Wang, C. & Yu, B. 2021a. Annual performance analysis of a dual-air-channel solar wall system with phase change material in different climate regions of China. Energy, 235. DOI: https://doi.org/10.1016/j.energy.2021.121359.

Ke, W., Ji, J., Xu, L., Yu, B., Tian, X. & Wang, J. 2021b. Numerical study and experimental validation of a multi-functional dual-air-channel solar wall system with PCM. Energy, 227. DOI: https://doi.org/10.1016/j.energy.2021.120434.

Li, A. & Ahmadi, G. 1993. Deposition of aerosols on surfaces in a turbulent channel flow. International Journal of Engineering Science, 31, 435-451. DOI: https://doi.org/10.1016/0020-7225(93)90017-O.

Liu, B. Y. & Agarwal, J. K. 1974. Experimental observation of aerosol deposition in turbulent flow. Journal of Aerosol Science, 5, 145-155. DOI: https://doi.org/10.1016/0021-8502(74)90046-9.

Liu, H., Liu, Z., He, J., Hu, C., Rong, R., Han, H., Wang, L. & Wang, D. 2023a. Reducing airborne transmission of SARS-CoV-2 by an upper-room ultraviolet germicidal irradiation system in a hospital isolation environment. Environ Res, 237, 116952. DOI: https://doi.org/10.1016/j.envres.2023.116952.

Liu, X., Qin, Z., Wang, L., Xie, X., Fu, Y., Yu, J., Liang, Z., He, X., Li, J. & Dai, H. 2023b. A simple and effective aerosol pathogen disinfection test for a flowing air disinfector. Journal of Biosafety and Biosecurity, 5, 32-38. DOI: https://doi.org/10.1016/j.jobb.2023.02.001.

Liu, Y., Ning, Z., Chen, Y., Guo, M., Liu, Y., Gali, N. K., Sun, L., Duan, Y., Cai, J. & Westerdahl, D. 2020. Aerodynamic analysis of SARS-CoV-2 in two Wuhan hospitals. Nature, 582, 557-560. DOI: https://doi.org/10.1038/s41586-020-2271-3.

Lu, H. & Lu, L. 2015. Numerical investigation on particle deposition enhancement in duct air flow by ribbed wall. Building and Environment, 85, 61-72. DOI: https://doi.org/10.1016/j.buildenv.2014.11.031.

Meng, H., Ji, J., Xie, H., Jia, H., Qian, Y., Li, J. & Mu, Y. 2025. Experimental study on the purification performance of sterilization-Trombe walls with and without fins in the heating season. Building and Environment, 277, 112948. DOI: https://doi.org/10.1016/j.buildenv.2025.112948.

Msemburi, W., Karlinsky, A., Knutson, V., Aleshin-Guendel, S., Chatterji, S. & Wakefield, J. 2023. The WHO estimates of excess mortality associated with the COVID-19 pandemic. Nature, 613, 130-137. DOI: https://doi.org/10.1038/s41586-022-05522-2.

Mullican, C. L., Buchanan, L. M. & Hoffman, R. K. 1971. Thermal inactivation of aerosolized Bacillus subtilis var. niger spores. Applied Microbiology, 22, 557-559. DOI: https://doi.org/10.1128/am.22.4.557-559.1971.

Pan, Y., Guo, K., Lin, C.-H., Wei, D., Ho, K.-F. & Chen, C. 2023. Developing a survival probability-based Lagrangian model for predicting ultraviolet disinfection of bioaerosols in enclosed environments. Building and Environment, 244. DOI: https://doi.org/10.1016/j.buildenv.2023.110765.

Phaiboun, A., Zhang, Y., Park, B. & Kim, M. 2015. Survival kinetics of starving bacteria is biphasic and density-dependent. PLoS computational biology, 11, e1004198. DOI: https://doi.org/10.1371/journal.pcbi.1004198.

Qian, Y., Ji, J., Xie, H., Jia, H., Meng, H., Li, J. & Mu, Y. 2024a. Performance comparison of multi-functional photovoltaic-Trombe wall with and without fins and their impacts on the removal of indoor infectious bioaerosols. Solar Energy, 282, 112854. DOI: https://doi.org/10.1016/j.solener.2024.112854.

Qian, Y., Ji, J., Xie, H., Jia, H., Meng, H., Li, J. & Mu, Y. 2024b. Performance investigation of multi-functional series-connected building-integrated photovoltaic/thermal system and analysis of its multi-objective optimization design strategy. Building and Environment, 112126. DOI: https://doi.org/10.1016/j.buildenv.2024.112126.

Qian, Y., Ji, J., Xie, H., Jia, H., Meng, H., Li, J. & Mu, Y. 2025a. Bi-level rolling optimal control method for air-purifying building-integrated photovoltaic thermal systems integrated with virtual energy storage. Energy Conversion and Management, 345. DOI: https://doi.org/10.1016/j.enconman.2025.120369.

Qian, Y., Ji, J., Xie, H., Jia, H., Meng, H., Li, J. & Mu, Y. 2025b. Research on dynamic operation strategy of heating, power generation, and air purification-type BIPVT system combined with machine learning. Energy, 334. DOI: https://doi.org/10.1016/j.energy.2025.137620.

Qian, Y., Ji, J., Xie, H., Jia, H., Tang, Y. & Mu, Y. 2024c. Performance prediction of a novel disinfection-enhanced type Trombe wall with transverse fins. Energy, 302, 131744. DOI: https://doi.org/10.1016/j.energy.2024.131744.

Reeks, M. 1977. On the dispersion of small particles suspended in an isotropic turbulent fluid. Journal of fluid mechanics, 83, 529-546. DOI: doi.org/10.1017/S0022112077001323.

Smolec, W. & Thomas, A. 1993. Theoretical and experimental investigations of heat transfer in a Trombe wall. Energy Conversion and Management, 34, 385-400. DOI: https://doi.org/10.1016/0196-8904(93)90089-S.

Song, L., Zhou, J., Wang, C., Meng, G., Li, Y., Jarin, M., Wu, Z. & Xie, X. 2022. Airborne pathogenic microorganisms and air cleaning technology development: A review. Journal of Hazardous Materials, 424, 127429. DOI: https://doi.org/10.1016/j.jhazmat.2021.127429.

Sun, W., Ji, J., Luo, C. & He, W. 2011. Performance of PV-Trombe wall in winter correlated with south façade design. Applied energy, 88, 224-231. DOI: https://doi.org/10.1016/j.apenergy.2010.06.002.

Tian, L. & Ahmadi, G. 2007. Particle deposition in turbulent duct flows—comparisons of different model predictions. Journal of Aerosol Science, 38, 377-397. DOI: https://doi.org/10.1016/j.jaerosci.2006.12.003.

Torres, Y. D., Herrera, H. H., Plasencia, M. A. A. G., Novo, E. P., Cabrera, L. P., Haeseldonckx, D. & Silva-Ortega, J. I. 2020. Heating ventilation and air-conditioned configurations for hotelsan approach review for the design and exploitation. Energy Reports, 6, 487-497. DOI: https://doi.org/10.1016/j.egyr.2020.09.026.

Van Boekel, M. A. 2002. On the use of the Weibull model to describe thermal inactivation of microbial vegetative cells. International journal of food microbiology, 74, 139-159. DOI: https://doi.org/10.1016/S0168-1605(01)00742-5.

Vlaskin, M. S. 2022. Review of air disinfection approaches and proposal for thermal inactivation of airborne viruses as a life-style and an instrument to fight pandemics. Applied Thermal Engineering, 202, 117855. DOI: https://doi.org/10.1016/j.applthermaleng.2021.117855.

Wang, C., Zhang, Z. W. & Liu, H. 2019. Microwave-induced release and degradation of airborne endotoxins from Escherichia coli bioaerosol. J Hazard Mater, 366, 27-33. DOI: https://doi.org/10.1016/j.jhazmat.2018.11.088.

Wu, S.-Y., Yan, R.-R. & Xiao, L. 2022. Numerically predicting the effect of fin on solar Trombe wall performance. Sustainable Energy Technologies and Assessments, 52. DOI: https://doi.org/10.1016/j.seta.2022.102012.

Xie, H., Jia, H., Ji, J., Qian, Y., Meng, H., Li, J. & Mu, Y. 2024a. Development and experimental validation of a thermal inactivation model for airborne bacteria and its application in Trombe wall systems. Building and Environment, 268, 112341. DOI: https://doi.org/10.1016/j.buildenv.2024.112341.

Xie, H., Jia, H., Ji, J., Qian, Y., Meng, H., Li, J. & Mu, Y. 2024b. Performance analysis of a novel air filtration and sterilization PV-Trombe wall. Building and Environment, 265, 111953. DOI: https://doi.org/10.1016/j.buildenv.2024.111953.

Xie, H., Yu, B., Wang, J. & Ji, J. 2021. A novel disinfected Trombe wall for space heating and virus inactivation: Concept and performance investigation. Applied Energy, 291, 116789. DOI: https://doi.org/10.1016/j.apenergy.2021.116789.

Xiong, R., Xie, G., Edmondson, A. & Sheard, M. 1999. A mathematical model for bacterial inactivation. International journal of food microbiology, 46, 45-55. DOI: https://doi.org/10.1016/S0168-1605(98)00172-X.

Yu, B., Li, N., Yan, C., Liu, X., Liu, H., Ji, J. & Xu, X. 2022. The comprehensive performance analysis on a novel high-performance air-purification-sterilization type PV-Trombe wall. Renewable Energy, 182, 1201-1218. DOI: https://doi.org/10.1016/j.renene.2021.11.029.

Yu, H., Tam, V. W. Y. & Xu, X. 2024. A systematic review of reinforcement learning application in building energy-related occupant behavior simulation. Energy and Buildings, 312, 14189. DOI: https://doi.org/10.1016/j.enbuild.2024.114189.

Zhao, B. & Chen, J. 2006. Numerical analysis of particle deposition in ventilation duct. Building and Environment, 41, 710-718. DOI: https://doi.org/10.1016/j.buildenv.2005.02.030.

Zhao, D., Ji, J., Yu, H., Wei, W. & Zheng, H. 2017. Numerical and experimental study of a combined solar Chinese kang and solar air heating system based on Qinghai demonstration building. Energy and Buildings, 143, 61-70. DOI: https://doi.org/10.1016/j.enbuild.2017.03.023.